Antiferromagnetic Resonance as a Tool for Investigating Magnetostructural Correlations: The Canted Antiferromagnetic State of $KMnPO_4 \cdot H_2O$ and a Series of Manganese Phosphonates

Gail E. Fanucci,[†] J. Krzystek,[§] Mark W. Meisel,[‡] Louis-Claude Brunel,[§] and Daniel R. Talham[†]*

Contribution from the Department of Chemistry and Department of Physics and Center for Ultralow-Temperature Research, University of Florida, Gainesville, Florida 32611, and Center for Interdisciplinary Magnetic Resonance, National High Magnetic Field Laboratory, Florida State University, Tallahassee, Florida 32310

Received December 15, 1997

Abstract: Antiferromagnetic resonance (AFMR) is used to characterize the canted antiferromagnetic state and to probe magnetostructural correlations within a series of layered solids including $KMnPO_4 \cdot H_2O$, four manganese alkylphosphonates, $Mn(O_3PC_nH_{2n+1}) \cdot H_2O$ ($n = 3-6$), and manganese phenylphosphonate. All samples were investigated as powders. A complete set of magnetic parameters, determined from AFMR and SQUID magnetometry, are presented for each material. The high field electron magnetic resonance facility at the National High Magnetic Field Laboratory in Tallahassee, Florida, was used to acquire AFMR spectra. Source frequencies ranged from 24 to 380 GHz, and the magnetic field range was 0−14.5 T. Correlations between the magnetic exchange and the electronic structure of the bridging ligand as well as measurements of the magnetic anisotropy in the ordered state are determined from analysis of the frequency and field dependence of the AFMR signals.

Introduction

Although first described in the 1950s,[1−4] antiferromagnetic resonance (AFMR) has remained a relatively unfamiliar and infrequently used technique in the field of chemistry.[5] AFMR provides a microscopic view of the magnetic structure in the ordered state, leading to measurements of magnetic exchange, magnetic anisotropy, spin-flop and critical fields, and spin canting. Although AFMR is potentially a very powerful tool, studies have long been restricted to a few materials with small exchange interactions because of the limited magnetic fields and microwave frequencies available with commercial electron paramagnetic resonance (EPR) instruments.[6] However, recent advances in instrumentation development, brought about by the availability of both larger magnets and microwave sources ranging up to several hundred gigahertz, now make possible investigations of a much larger range of antiferromagnetically ordered materials.[7−12] Currently, neutron diffraction and static magnetometry measurements are commonly used to obtain similar information about the magnetic structure and the spin exchange interactions in the ordered state. AFMR compliments these two techniques, but at the same time it offers some substantial advantages. Unlike neutron diffraction, deuteration of the sample is unnecessary for AFMR, typically 100 mg of material affords sufficient signal-to-noise, and analysis of the data does not involve intensive computational methods. In addition, AFMR provides values of the anisotropy of the magnetic interactions that are not always easily determined from static magnetometry measurements. AFMR can be performed on both powdered samples and single crystals, and when single crystals are available, this technique can be used to assign the relationship between the principal crystallographic axes and the magnetic axes. The AFMR method is straightforward, making it feasible to study a series of materials for the purpose of obtaining magnetostructural comparisons.

In this article, we demonstrate how AFMR can be used to probe magnetostructural correlations by investigating a series of related layered antiferromagnets that includes the purely inorganic $KMnPO_4 \cdot H_2O$, manganese phenylphosphonate [$Mn(O_3PC_6H_5) \cdot H_2O$], and four manganese alkylphosphonates [$Mn(O_3PC_nH_{2n+1}) \cdot H_2O$; $n = 3-6$]. The metal phosphonates are a class of mixed organic−inorganic layered solids where metal ions, bridged by the phosphonate groups, form sheets that are separated from one another by the organic substituents of the

* To whom correspondence should be addressed.
[†] Department of Chemistry.
[‡] Department of Physics and Center for Ultralow-Temperature Research.
[§] Center for Interdisciplinary Magnetic Resonance.

(1) Kittel, C. *Phys. Rev.* **1951**, *82*, 565.
(2) Keffer, F.; Kittel, C. *Phys. Rev.* **1952**, *85*, 329−337.
(3) Nagamiya, T. *Prog. Theor. Phys.* **1954**, *11*, 209−327.
(4) Nagamiya, T.; Yosida, K.; Kubo, R. *Adv. Phys.* **1955**, *4*, 1−112.
(5) Goodenough, J. B. *Magnetism and the Chemical Bond*; John Wiley & Sons: New York, 1966; p 393.
(6) Foner, S. In *Magnetism*; Rado, G. T., Suhl, H., Eds.; Academic: 1963; Vol. 1; pp 383−447.
(7) Hagiwara, M.; Katsumata, K.; Tuchendler, J. *J. Phys.: Condens. Matter* **1994**, *6*, 545−550.
(8) Katsumata, K.; Tuchendler, J. *J. Phys. C: Solid State Phys.* **1987**, *20*, 4873−4879.
(9) Ohta, H.; Yamauchi, N.; Nanba, T.; Motokawa, M.; Kawamata, S.; Okuda, K. *J. Phys. Soc. Jpn.* **1993**, *62*, 785−792.
(10) Ohta, H.; Yoshida, K.; Matsuya, T.; Nanba, T.; Motokawa, M.; Yamada, K.; Endoh, Y.; Hosoya, S. *J. Phys. Soc. Jpn.* **1992**, *61*, 2921−2929.
(11) Ohta, H.; Kimura, S.; Motokawa, M. *J. Phys. Soc. Jpn.* **1995**, *64*, 3934−3940.
(12) Ohta, H.; Sumikawa, M.; Motokawa, M.; Noro, S.; Yamadaya, T. *J. Phys. Soc. Jpn.* **1995**, *64*, 1759−1765.

S0002-7863(97)04247-9 CCC: $15.00
Published on Web 05/20/1998

phosphonate ligands. Layered structures form with a variety of divalent,[13−17] trivalent,[18−20] and tetravalent[21−23] metal ions and with a range of organophosphonate ligands.[22,24−28] The ability to pillar and intercalate[29−32] the layers has stimulated interest in these materials related to uses as catalysts, sorbents, and ion-exchangers. Metal phosphonates have also attracted the attention of those interested in magnetic interactions in low-dimensional solids,[33] partially because of the relationship of layered antiferromagnets to layered superconductors.[9,11] The metal phosphonates provide a class of layered magnetic materials where magnetic interactions can be varied through changes in either the inorganic or the organic components of the solids.[34−37]

The structures of the divalent metal organophosphonates (where M^{II} = Mn, Ni, Co, Fe) are analogs to the metal phosphate hydrates, $M^{I}M^{II}PO_4 \cdot H_2O$ (M^{I} = K, NH_4; M^{II} = Mn, Ni, Co, Fe), which were reported by Bassett and Bedwell[38] in 1933. The purely inorganic analogues crystallize in the orthorhombic space group P$mn2_1$, and their structures consist of approximately square planar sheets of M^{II} ions that are coordinated in a severely distorted octahedron by five phosphate oxygens and one water molecule, with the layers separated by the M^{I} ions. The metal organophosphonates have a similar in-plane metal phosphonate extended layer (Figure 1) and also crystalize in the P$mn2_1$ space group, but now the M^{II} planes are separated by the organic pendant groups.[13,15]

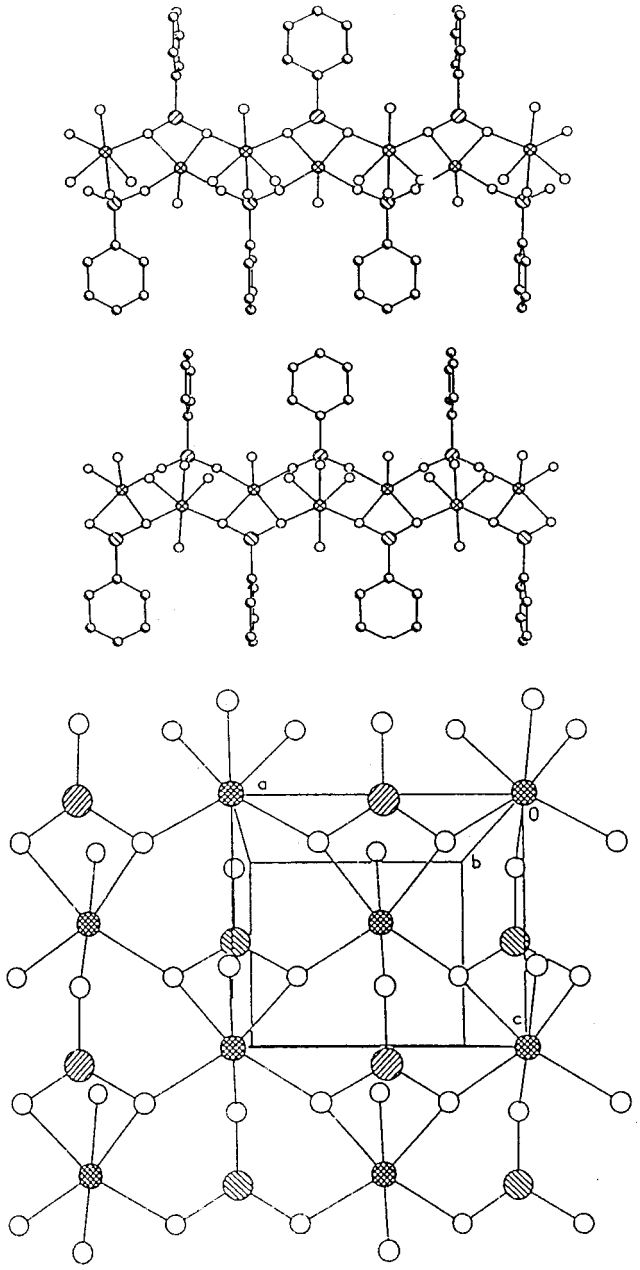

Figure 1. Illustration of the layered structure of $Mn(O_3PC_6H_5)\cdot H_2O$ (top) and the manganese ion plane viewed perpendicular to the layer where the phenyl groups have been omitted for clarity (bottom). Each manganese ion is coordinated by five phosphonate oxygens and one water molecule. Figures were generated from crystallographic data taken from ref 13. Key: oxygen, small open circles; manganese, crosshatched circles; phosphorus, diagonal-hatched circles (phosphorus atoms above and below the plane are distinguished by hatch marks with different directions).

Carling et al.[39] have shown, with magnetometry measurements, that the magnetic properties of $KMnPO_4\cdot H_2O$ and the manganese alkylphosphonates [$Mn(O_3PC_nH_{2n+1})\cdot H_2O$; n = 1−4] are well described as 2-dimensional layers of S = 5/2 manganese ions with Heisenberg antiferromagnetic nearest-neighbor exchange, and that each material orders antiferromagnetically between 12 and 19 K. Although nearest neighbor exchange is antiferromagnetic, below the ordering temperature the equilibrium distribution of moments is not collinear, but

(13) Cao, G.; Lee, H.; Lynch, V. M.; Mallouk, T. E. *Inorg. Chem.* **1988**, *27*, 2781−2785.
(14) Cao, G.; Lee, H.; Lynch, V. M.; Mallouk, T. E. *Solid State Ionics* **1988**, *26*, 63−69.
(15) Bujoli, B.; Pena, O.; Palvadeau, P.; Le Bideau, J.; Payen, C.; Rouxel, J. *Chem. Mater.* **1993**, *5*, 583−587.
(16) Cunningham, D.; Hennelly, P. J. D. *Inorg. Chim. Acta* **1979**, *37*, 95−102.
(17) Ortiz-Avila, Y.; Rudolf, P. R.; Clearfield, A. *Inorg. Chem.* **1989**, *28*, 2137−2141.
(18) Bujoli, B.; Palvadeau, P.; Rouxel, J. *Chem. Mater.* **1990**, *2*, 582−589.
(19) Cao, G.; Lynch, V. M.; Swinnea, J. S.; Mallouk, T. E. *Inorg. Chem.* **1990**, *29*, 2112−2117.
(20) Wang, R.-C.; Zhang, Y.; Hu, H.; Frausto, R. R.; Clearfield, A. *Chem. Mater.* **1992**, *4*, 864−870.
(21) Poojary, M. D.; Hu, H.; Campbell, I., F. L.; Clearfield, A. *Acta Crystallographica B* **1993**, *49*, 996.
(22) Cao, G.; Hong, H.-G.; Mallouk, T. E. *Acc. Chem. Res.* **1992**, *25*, 420−427.
(23) Clearfield, A.; Smith, G. D. *Inorg. Chem.* **1969**, *8*, 431−436.
(24) Katz, H. E.; Schilling, M. L.; Chidsey, C. E. D.; Putvinski, T. M.; Hutton, R. S. *Chem. Mater.* **1991**, *3*, 699−703.
(25) Katz, H. E.; Scheller, G.; Putvinski, T. M.; Schilling, M. L.; Wilson, W. L.; Chidsey, C. E. D. *Science* **1991**, *254*, 1485−1487.
(26) Katz, H. E.; Wilson, W. L.; Scheller, G. *J. Am. Chem. Soc.* **1994**, *116*, 6636−6640.
(27) Dines, M. B.; DiGiacomo, P. M. *Inorg. Chem.* **1981**, *20*, 92−97.
(28) Poojary, D. M.; Vermeulen, L. A.; Vicenzi, E.; Clearfield, A.; Thompson, M. E. *Chem. Mater.* **1994**, *6*, 1845−1849.
(29) Drumel, S.; Janvier, P.; Barboux, P.; Bujoli-Doeff, M.; Bujoli, B. *Inorg. Chem.* **1995**, *34*, 148−156.
(30) Zhang, Y.; Scott, K. J.; Clearfield, A. *Chem. Mater.* **1993**, *5*, 495−499.
(31) Frink, K. J.; Wang, R.; Colón, J. L.; Clearfield, A. *Inorg. Chem.* **1991**, *30*, 1438−1441.
(32) Cao, G.; Lynch, V. M.; Yacullo, L. N. *Chem. Mater.* **1993**, *5*, 1000−1006.
(33) *Organic and Inorganic Low-Dimensional Crystalline Materials*; Plenum: New York, 1987; Vol. Series B: Physics Vol. 168, p 482.
(34) Carling, S. G.; Day, P.; Visser, D.; Kremer, R. K. *J. Solid State Chem.* **1993**, *106*, 111−119.
(35) Carling, S. G.; Day, P.; Visser, D. *J. Phys.: Condens. Matter* **1995**, *7*, L109−L113.
(36) Le Bideau, J.; Payen, C.; Bujoli, B.; Palvadeau, P.; Rouxel, J. *J. Magn. Magn. Mater.* **1995**, *140−144*, 1719−1720.
(37) Le Bideau, J.; Papoutsakis, D.; Jackson, J. E.; Nocera, D. *J. Am. Chem. Soc.* **1997**, *119*, 1313−1316.
(38) Besset, H.; Baldwell, W. L. *J. Chem. Soc.* **1933**,.
(39) Visser, D.; Carling, S. G.; Day, P.; Deportes, J. *J. Appl. Phys.* **1991**, *69*, 6016−6018.

Scheme 1. Representation of the Magnetization Vectors in an Ordered Antiferromagnetic State and in an Ordered Canted Antiferromagnetic State

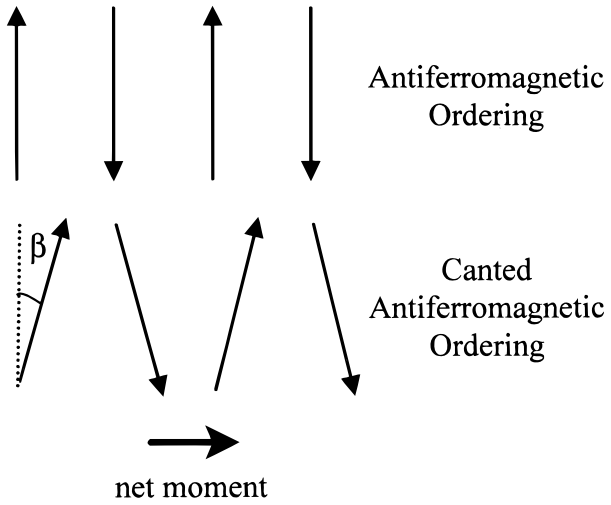

Scheme 2. Representation of the Antiferromagnetic Structure of the Mn ($S = 5/2$) Spins in the Ternary Metal Phosphates[40] as Determined from Powdered Neutron Diffraction Measurements[a]

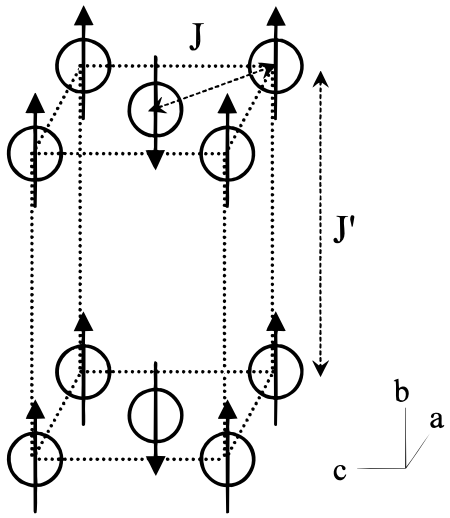

[a] Canting angles are not included in this representation because the value of β is too small to be observed in the neutron data.

canted from the magnetic easy-axis, producing a spontaneous magnetization[34,40] (Scheme 1). Such systems are known as canted antiferromagnets or "weak ferromagnets". Neutron diffraction studies of $ND_4MnPO_4 \cdot D_2O$ and $KMnPO_4 \cdot D_2O$ have determined that in the inorganic solids the magnetic and chemical unit cells are coincident and the magnetic easy-axis lies perpendicular to the metal plane along the crystallographic *b*-axis (Scheme 2).[40] Although symmetry considerations require that the canted moment lies within the metal plane, the magnitude of the canting angle is too small to be resolved from the neutron data.[40] Although the magnetic structures of the manganese organophosphonates have not yet been determined, the magnitude of the spontaneous magnetization moment is similar to that in the inorganic phosphates. In addition, for Langmuir−Blodgett films of manganese octadecylphosphonate, $Mn(O_3PC_{18}H_{37}) \cdot H_2O$, SQUID magnetometry has shown that the manganese $S = 5/2$ moments are aligned perpendicular to the metal planes and that the "weak ferromagnetic" moment lies within the metal plane.[41]

A microscopic characterization of the ordered state of the divalent organophosphonates has not yet been achieved because of the difficulty in obtaining large amounts of the deuterated solids needed for neutron diffraction studies. On the other hand, the polycrystalline powders of the hydrogenated metal organophosphonates that are normally obtained when preparing these materials are well suited to the AFMR experiments. To learn more about the canted antiferromagnetic state of the manganese phosphonates and to demonstrate the potential utility of the AFMR technique for obtaining magnetostructural correlations, we have studied several manganese organophosphonates and the inorganic $KMnPO_4 \cdot H_2O$ by AFMR. The AFMR measurements reported here were acquired with the high field electron magnetic resonance (EMR) instrument at the National High Magnetic Field Laboratory (NHMFL). After a brief review of background pertaining to antiferromagnetism and antiferromagnetic resonance, the AFMR and SQUID magnetometry results are presented and analyzed, giving a complete set of magnetic parameters for each material. Correlations are made between the observed magnetic behavior and the electronic structure of the bridging ligand as it changes from a phosphate to an alkylphosphonate to a phenylphosphonate group. Differences in the magnetic parameters among the manganese organophosphonates are also quantified.

Background

Antiferromagnetism. The ordered state of an antiferromagnet is characterized by an arrangement of magnetic moments that are aligned antiparallel to one another.[42] This arrangement can be represented by two interpenetrating sublattices, where each sublattice consists of spins of the same magnitude aligned parallel to one another and where the two sublattices have equal magnetization but are arranged in an antiparallel fashion (Scheme 1). The direction parallel to the spin alignment is termed the magnetic easy-axis.

The interactions between nearest-neighbor spins are treated by mean-molecular field theory (MFT) as an effective internal magnetic field.[42] This effective internal field can be represented as an exchange field, H_E, which indicates how strongly the nearest-neighbors spins interact with each other, and as anisotropy fields, H_{A1} and H_{A2}, which give an indication of how the magnetic interactions vary as a function of orientation with respect to the magnetic principal axes. The anisotropy fields can be thought of as the sum of all internal factors that contribute to the lack of ideal isotropic magnetic interactions, with the most important quantities being single-ion interactions, such as dipole−dipole or crystal field interactions, and anisotropic exchange interactions, such as spin−orbit coupling effects. A distinction can be made between a uniaxial antiferromagnet, where $H_{A1} = H_{A2}$, and an orthorhombic antiferromagnet where $H_{A1} \neq H_{A2}$. For a uniaxial antiferromagnet, the magnetic interactions perpendicular to the magnetic easy-axis are isotropic, whereas for an orthorhombic antiferromagnet, the magnetic interactions in the plane perpendicular to the magnetic easy-axis are anisotropic.

In the ordered state of antiferromagnetic materials, a phenomenon termed spin-flop is observed when an applied magnetic field aligned parallel to the magnetic easy-axis exceeds a critical

(40) Carling, S. G.; Day, P.; Visser, D. *Inorg. Chem.* **1995**, *34*, 3917−3927.

(41) Seip, C. T.; Granroth, G. E.; Meisel, M. W.; Talham, D. R. *J. Am. Chem. Soc.* **1997**, *119*, 7084−7094.

(42) Carlin, R. L. *Magnetochemistry*, 1st ed.; Springer-Verlag: Berlin, 1986.

value termed the spin-flop field, H_{SF},[6,42] which is dependent on the values of H_E, H_{A1}, and H_{A2}. For a uniaxial antiferromagnet the expression for the spin-flop field at 0 K is given by[42] $H_{SF} = [2H_EH_A - H_A^2]^{1/2}$. Immediately above this critical field, the direction of spin alignment will 'flop' to an orientation that is perpendicular to that of the original magnetic easy-axis, giving rise to a new phase called the spin-flop state.

The materials investigated in this paper are known to be canted antiferromagnets. In a canted antiferromagnet, the sublattice magnetic moments are not collinear with each other, but canted slightly from the magnetic easy-axis (Scheme 1). This small perturbation from the antiferromagnetic state can be considered in the MFT approximation by an additional effective field, H_{D-M}, called the Dzyaloshinsky-Moriya[43,44] interaction, which is discussed in greater detail later in the text.

Antiferromagnetic Resonance (AFMR). AFMR is a type of EMR that occurs in the ordered state of antiferromagnetic materials and can be described by principles similar to those used to represent nuclear magnetic resonance (NMR).[6,45] In the ordered antiferromagnetic state, the sublattice magnetic moments can be thought of as precessing about an equilibrium position. The effective internal magnetic field and the applied magnetic field act as forces that produce torques on the magnetic moments resulting in a precessional motion of the spins. The AFMR signals can be detected experimentally when the applied excitation source frequency equals the precessional frequency. Even in the absence of an applied external field, the presence of the internal fields results in a dynamic response, and this precessional frequency is referred to as the zero-field resonance. For an orthorhombic antiferromagnet there are two zero-field resonance frequencies, whereas in the uniaxial case, these two resonances are degenerate because $H_{A1} = H_{A2}$.

Applied external fields act as additional effective fields that modify the precessional frequency, and hence, the frequency of the observed AFMR signals from the zero-field values. The frequency of the detected AFMR signal will also depend on the orientation of the applied magnetic field with respect to the magnetic principal axes.[46,47] Because of this orientational dependence, in a powdered sample where all possible orientations are represented equally, the AFMR signals corresponding to the modes of the three magnetic principal axes can be observed simultaneously (this is best observed when spectra are recorded as dervatives of the absorbance signals). For example, consider first the modes that originate from fields applied perpendicular to the magnetic easy-axis. For an orthorhombic antiferromagnet, there will be two signals, one from each perpendicular direction, whereas in a uniaxial antiferromagnet, these two modes are degenerate, leading to the observation of only one signal. The number of signals arising from the application of an applied field that is parallel to the magnetic easy axis does not differ for the uniaxial and orthorhombic antiferromagnet. When the applied field has a value $> H_{SF}$, one signal from the spin-flop state can be detected. For parallel applied fields that have values $< H_{SF}$, two parallel modes are observed, and these result as a consequence of two interpenetrating sublattices.[6] Therefore, for the parallel orientation, the value of the applied external magnetic field determines whether one or two AFMR signals are present; on the other hand, the number of perpendicular modes is determined by the presence or absence of in-plane anisotropy. The frequency dependence of the AFMR signals on the applied field for the specific case of a uniaxial antiferromagnet and for the general case of an orthorhombic antiferromagnet have been considered by Keffer and Kittel,[1,2] Nagamiya and Yosida,[3,4] and others.[48,49] Because the precessional frequencies of each mode, and hence the AFMR signals, depend on both the applied fields and internal fields such as H_E, H_{A1}, H_{A2}, and H_{D-M}, analysis of the frequency and field dependence of the AFMR signals of each of these modes gives information about the magnetic interactions of the ordered state.

In addition to MFT, the spin-Hamiltonian formalism of superexchange is often used to describe interactions between nearest-neighbor spins. The spin-Hamiltonian for metal−metal exchange interactions in magnetic insulators[50] is of the form $H = -\Sigma J_{ij}S_iS_j$, where the sum is taken over all nearest neighbor pairwise interactions. A negative value of J indicates antiferromagnetic exchange, and the magnitude of J indicates how strongly the spins interact with each other. By noting that S_i and S_j are vectors, the anisotropy of the exchange interaction can be represented by the components $J_\alpha S_{ix}S_{jx}$, $J_\beta S_{iy}S_{jy}$, and $J_\gamma S_{iz}S_{jz}$. Single-ion anisotropy interactions, such as crystal field interactions or magnetic dipole interactions, can be introduced by additional terms in the spin-Hamiltonian, typically of the form[51] $-D\Sigma(S_{ix})^2$ and $E\Sigma[(S_{iz})^2 - (S_{iy})^2]$. Although most of the investigations of AFMR use the MFT formulation to interpret AFMR data, the mean field parameters H_E, H_{A1}, and H_{A2} can be related to the spin-Hamiltonian formalism of magnetic interactions. The exchange field, H_E, in MFT is related to J and the number of nearest neighbor spins, and the anisotropy fields, H_{A1} and H_{A2}, are a combination of the anisotropy in the exchange and the single-ion anosotropy terms.

Experimental Section

Materials and Methods. Reagents used were of reagent grade quality and were obtained from commercial sources. Pentyl- and hexylphosphonic acid were prepared by literature procedures,[52,53] and all other alkyl- and arylphosphonic acids were purchased from Aldrich (Milwaukee, WI). Deionized water was purified with a Barnstead NANOpure (Boston, MA) system. Syntheses of powdered metal phosphonates have been described in detail elsewhere.[13,14,16] Elemental analyses were consistent with the formulas $Mn(O_3PC_nH_{2n+1})\cdot H_2O$ ($n = 3-6$) for alkylphosphonates and $Mn(O_3PC_6H_5)\cdot H_2O$ for the phenyl phosphonate. The ternary metal phosphate hydrate, $KMnPO_4\cdot H_2O$, was prepared by published methods.[38,40]

Magnetization measurements were performed using a Quantum Design MPMS SQUID magnetometer. A gel cap and plastic straw were used as a sample holder during the measurements. Background signals arising from the gel cap and straw were minimal and not subtracted from the reported data because the background contribution represented <0.1% of the observed signal intensity. Magnetization versus field measurements were performed at 2 and 5 K by sweeping the field both up and down over the range of 0 to 5 T. Magnetization versus temperature measurements were run from 2 to 300 K. Samples were first cooled in the absence of an applied field and the magnetization was then measured on warming between 2 and 300 K in an applied field of 0.1 T to give the zero-field cooled data. Field cooled data

(43) Dzyaloshinsky, I. *J. Phys. Chem. Solids* **1958**, *4*, 241−255.
(44) Moriya, T. *Phys. Rev.* **1960**, *120*, 91−98.
(45) Kittel, C. *Introduction to Solid State Physics*, 6th ed.; John Wiley & Sons: New York, 1986.
(46) Yoshioka, H.; Saiki, K. *J. Phys. Soc. Jpn.* **1972**, *33*, 1566−1573.
(47) Saiki, K. *J. Phys. Soc. Jpn.* **1972**, *33*, 1284−1291.
(48) Date, M. *J. Phys. Soc. Jpn.* **1961**, *16*, 1337−1351.
(49) Date, M.; Nagata, K. *J. Appl. Phys.* **1963**, *34*, 1038−1044.
(50) de Jongh, L. J. In *Magnetic Properties of Layered Transition Metal Compounds*; de Jongh, L. J., Ed.; Kluwer Academic: Dordrecht, 1990; pp 1−51.
(51) This treatment follows the presentation in ref 50, but here the magnetic easy-axis is denoted by the x-direction in an attempt to be consistent with the formalsim of AFMR theory.
(52) Tavs, P. *Chem. Ber.* **1970**, *103*, 2428.
(53) Grabiak, R. C.; Miles, J. A.; Schwenzer, G. M. *Phosphorus Sulfur* **1980**, *9*, 197−202.

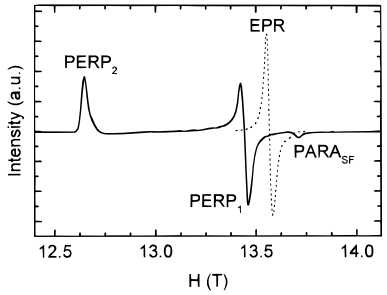

Figure 2. EPR and AFMR spectra with source frequency of 380.84 GHz for manganese pentylphosphonate. The AFMR spectrum, solid line, was recorded at 5 K, whereas the EPR spectrum, dashed line, was recorded at room temperature. Both spectra were recorded as upfield sweeps. The AFMR modes are discussed in the text.

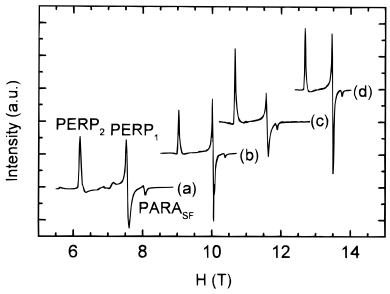

Figure 3. AFMR spectra detected for manganese pentylphosphonate at 5 K with source frequencies of (a) 218.18 GHz, (b) 285.42 GHz, (c) 330.37 GHz, and (d) 380.84 GHz, all with upfield sweeps.

were acquired by cooling the sample from 300 K in 0.1 T and measuring the magnetization from 2 to 300 K in the same 0.1 T applied field.

EPR and AFMR Measurements. All EPR and AFMR measurements were performed on powdered samples, and spectra were acquired using the high-field EMR facility at the NHMFL in Tallahassee, Florida. The EMR spectrometer design is similar to that described earlier by Mueller et al.,[54] with the following modifications. Two different types of millimeter and submillimeter wave radiation sources were used. Two Gunn oscillators were used (AB Millimeter, Paris) to access higher frequencies (95−380 GHz); one was tunable over the range 92−98 GHz and the other over the range 108−112 GHz. In addition to operating at the fundamental frequencies, these Gunn sources were equipped with sets of Schottky-diode harmonic generators and filters that enabled operation at frequencies near 190, 285, and 380 GHz for the low-frequency oscillator, as well as 220 and 330 GHz for the higher frequency Gunn source. A second type of source, a Millimeter Vector Network Analyzer (MVNA) produced continuous fundamental frequencies of 8−18 GHz. Equipped with a series of Schottky-diode harmonic generators, the MVNA provided an essentially continuous source from 24 to 133 GHz, where the lower end was limited by the detector sensitivity. The frequency was measured by an EIP 578B counter that was also used as a frequency lock source for the Gunn oscillators and the MVNA. The Zeeman field was produced by an Oxford Instruments Teslatron superconducting magnet capable of field sweeps from 0 to 17 T. The resonance absorption was measured at a fixed frequency by monitoring the transmitted power as a function of the applied magnetic field that is swept through the resonance with either an increasing or decreasing field. Because the signals were broad, a relatively fast sweep rate, typically 0.2 T/min was used. This rate resulted in a hysteresis of the magnetic field as read by the power supply current. To account for this hysteresis, typically 0.02 T, resonance fields are reported as the average of the signals detected in an upfield and downfield sweep. The field was modulated in the usual fashion with a frequency of 4−10 kHz, and phase detection was employed. A liquid helium cooled hot-electron InSb bolometer from QMC (London, England) was used as the power detector. All AFMR measurements were performed at 5 K, and the EPR spectra were taken over the range 20−285 K, each with an Oxford Instruments CF-1200 continuous flow liquid helium cryostat. Typical powder sample sizes were 20−30 mg when the Gunn oscillators were used as sources, and 100−200 mg when MVNA was used as the source. Samples were ground into fine powders to ensure equal representation of all orientations.

Results

For all samples, as the temperature is decreased the EPR signals broaden, and below the ordering temperature, T_N, the EPR signals disappear and the AFMR signals appear and intensify. Figure 2 gives representative spectra of the EPR signal at room temperature and the AFMR signals observed at 5 K for a powder of manganese pentylphosphonate, $Mn(O_3PC_5H_{11})\cdot H_2O$. As shown in Figure 2, with an excitation source frequency of 380.84 GHz, the EPR signal occurs at 13.57 ± 0.01 T and the value of the *g*-factor is 2.00 ± 0.03.[55] For frequencies of 95 to 380 GHz, no anisotropy of the *g*-factor was apparent in the EPR signals for any of the samples studied. Below T_N, three new resonance modes are clearly observed in the AFMR spectrum, as shown in Figure 2. The signal at lowest field, 12.65 ± 0.02 T, corresponds to the perpendicular mode where the applied field is along the direction of the net canted moment, labeled $PERP_2$. The next signal, at 13.45 ± 0.02 T, arises from the other perpendicular orientation, $PERP_1$, and the last signal at 13.71 ± 0.02 T, designated $PARA_{SF}$, is the mode where the applied field is parallel to the magnetic easy-axis and has values larger than the spin-flop field, H_{SF}. For excitation source frequencies of the higher harmonics of the 95 and 110 GHz Gunn oscillators, a similar pattern of three signals is detected for all six samples. The presence of two perpendicular modes is characteristic of an orthorhombic antiferromagnet, and the pronounced splitting between these two modes is indicative of large in-plane anisotropy. The zero-field resonance frequencies for the two perpendicular modes differed by ∼60 GHz for each of the materials studied.

Figure 3 shows AFMR spectra acquired for manganese pentylphosphonate at several frequencies. It is clear from this figure how the resonance field of each of the three signals changes as a function of source frequency. This dependence is depicted in Figure 4, which summarizes in the frequency and field plane the AFMR signals detected for (A) $KMnPO_4\cdot H_2O$, (B) manganese phenylphosphonate, (C) manganese propylphosphonate, (D) manganese butylphosphonate, (E) manganese pentylphosphonate, and (F) manganese hexylphosphonate. The solid lines are fits to available theory and will be discussed in greater detail later. Each data point in the frequency and field plane represents an observed AFMR signal of the types shown in Figures 2 and 3.

Data points in the frequency and field area of 30−130 GHz and 0−5 T were acquired with the MNVA source with appropriate Schottky-diode harmonic generators. Figure 5 shows typical AFMR signals for manganese hexylphosphonate detected with this source at 5 K. The signal at 1.36 ± 0.04 T for a source frequency of 50.24 GHz in Figure 5A belongs to the parallel branch below the spin-flop field. The small signal at 2.1 ± 0.1 T, as well as that at 2.0 ± 0.1 T in Figure 5B, indicate the field at which spin-flop occurs, H_{SF}.[6] Figure 5B shows signals originating from the parallel orientation for fields

(54) Mueller, F.; Hopkins, M. A.; Coron, N.; Grynberg, M.; Brunel, L. C.; Martinez, G. *Rev. Sci. Instr.* **1989**, *60*, 3681.

(55) The reader is reminded that spectra, such as those in Figures 2 and 3, are actual data recorded with either an upfield or downfield sweep. The resonance field values reported in the text correspond to the actual spectra, whereas the resonance field values plotted in Figure 4 and the values of the reported *g*-factor represent the average value determined from both an upfield and downfield sweep.

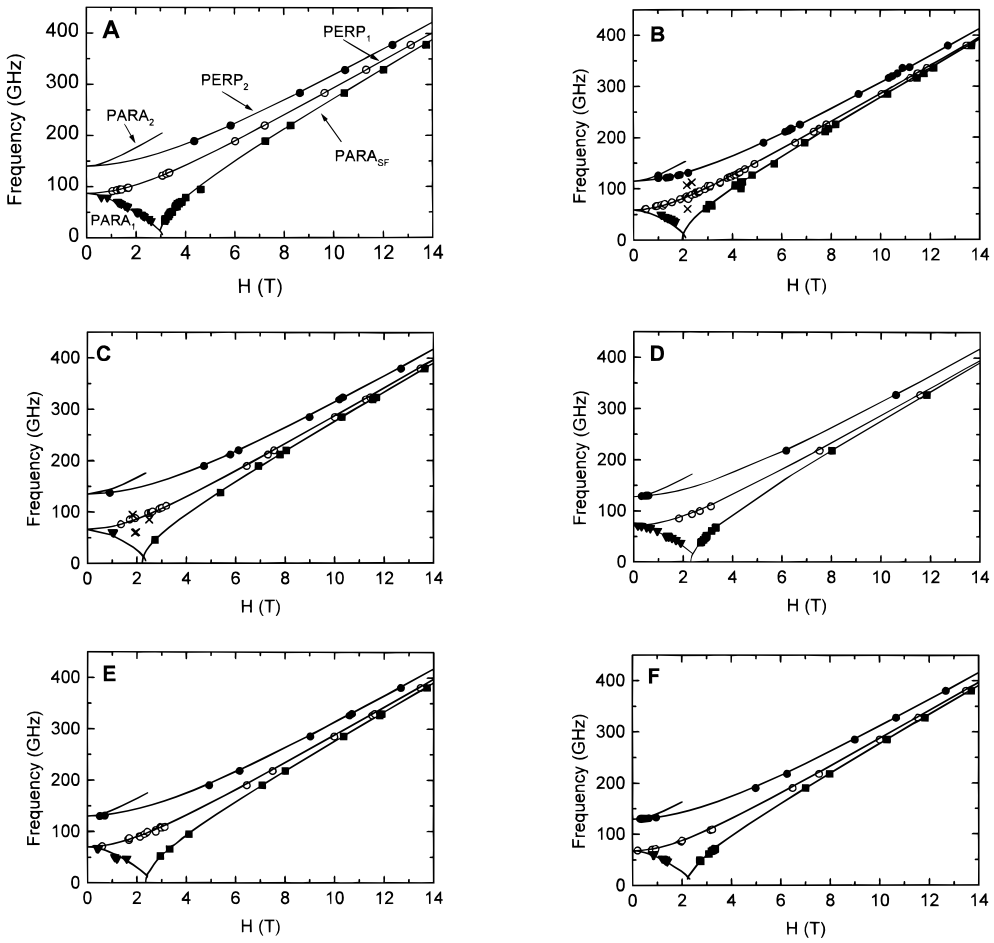

Figure 4. Frequency and field dependence of the AFMR signals detected for (A) $KMnPO_4 \cdot H_2O$, (B) manganese phenylphosphonate, (C) manganese propylphosphonate, (D) manganese butylphosphonate, (E) manganese pentylphosphonate and (F) manganese hexylphosphonate at 5 K. The solid lines are fits to conventional theory as described in the text. The various signal origins are depicted as follows: solid circles, $PERP_2$; open circles, $PERP_1$; solid triangles, $PARA_1$($H_o < H_{SF}$); solid squares, $PARA_{SF}$ ($H_o > H_{SF}$); crosshatches, H_{SF}. Each resonance field represents the average of the signals detected in an upfield and downfield-sweep. Mode assignments are discussed in detail in the text.

Table 1. Magnetic Parameters Determined from SQUID Magnetometry Measurements

sample	T_N (K)	$T_{\chi max}$ (K)	J (K)	C(cgs)[a]	θ (K)[b]	μ_{eff}/μ_β	μ_{ferro}/μ_β	α (deg)[c]	H_{SF} (T)[d]
$KMnPO_4 \cdot H_2O$[e]	18.40 (2)	29.8 (4)	−3.32 (6)	3.56 (1)	−62.7 (3)	5.36 (1)	3.5e-3 (3)	0.03 (1)	3.2 (1)
$Mn(O_3PC_6H_5) \cdot H_2O$[f]	12.1 (1)	19 (1)	−2.2 (2)	4.56 (1)	−46 (1)	6.00 (3)	NA[g]	NA[g]	2.4 (2)
$Mn(O_3PC_3H_7) \cdot H_2O$[h]	14.90 (2)	22.4 (4)	−2.48 (8)	3.68 (1)	−51.7 (4)	5.45 (1)	0.0143 (1)	0.15 (1)	2.6 (2)
$Mn(O_3PC_4H_9) \cdot H_2O$[h]	15.00 (2)	22.4 (4)	−2.48 (6)	3.68 (1)	−54.49 (3)	5.45 (1)	0.0278 (1)	0.29 (1)	2.5 (1)
$Mn(O_3PC_5H_{11}) \cdot H_2O$	14.65 (2)	25.5 (3)	−2.85 (4)	3.83 (3)	−48.9 (1)	5.67 (3)	0.0438 (2)	0.44 (2)	2.5 (2)
$Mn(O_3PC_6H_{13}) \cdot H_2O$	14.10 (2)	24.0 (3)	−2.65 (4)	3.99 (3)	−56.1 (1)	5.91 (3)	0.0553 (2)	0.54 (2)	2.3 (2)

[a] Curie constant. [b] Weiss constant. [c] α is the canting angle determined from bulk magnetization measurements, $\sin^{-1}\alpha = \mu_{ferro}/\mu_{eff}$ (ref 35). [d] H_{SF} values for all samples have been determined from our measurements. [e] Data taken from ref 40. [f] Data taken from ref 36. [g] Values not reported in ref 36. [h] Data taken from ref 35.

both below and above H_{SF}, occurring at 0.21 ± 0.04 and 3.29 ± 0.04 T, respectively. In Figure 5C, the signal at 0.25 ± 0.04 T for source frequency of 130.23 GHz originates from the perpendicular direction ($PERP_2$), along which the canted moment lies.

When using the MVNA source, assignment of the frequencies of the AFMR signals was sometimes complicated by more than one harmonic of the fundamental frequency passing through the system. To aid in the assignments, scans were taken above T_N (typically 25 K for the organophosphonates and at 35 K for $KMnPO_4 \cdot H_2O$) and below T_N for each fundamental frequency run with a given harmonic generator. This procedure identified which harmonics of the fundamental frequencies were present as excitation sources in the AFMR spectra. When more than one frequency was present, modes were assigned by slightly changing the fundamental frequency and watching which way the AFMR signal(s) shifted. Signals belonging to the lower parallel mode, for applied fields $< H_{SF}$ (mode assignments are discussed in more detail later), move to lower field with higher frequency, whereas all other modes shift to higher field as the frequency is increased. The progression of the AFMR signals of the $PARA_1$ and $PARA_{SF}$ modes as a function of frequency can be observed in Figure 6 for $KMnPO_4 \cdot H_2O$. For example, as the frequency increases from 36.32 to 61.05 GHz, the signals belonging to the $PARA_1$ mode move from 2.52 ± 0.04 to 1.81 ± 0.04 T (shown by the solid triangles in Figure 4A), whereas the signals due to the parallel orientation once spin-flop has occurred ($PARA_{SF}$) move from 3.2 ± 0.1 to 3.6 ± 0.1 T in Figure 6 (shown by the solid squares in Figure 4A).

Spin-flop fields were determined from analysis of the frequency versus field dependence of the AFMR signals as well as from SQUID magnetometry magnetization versus field

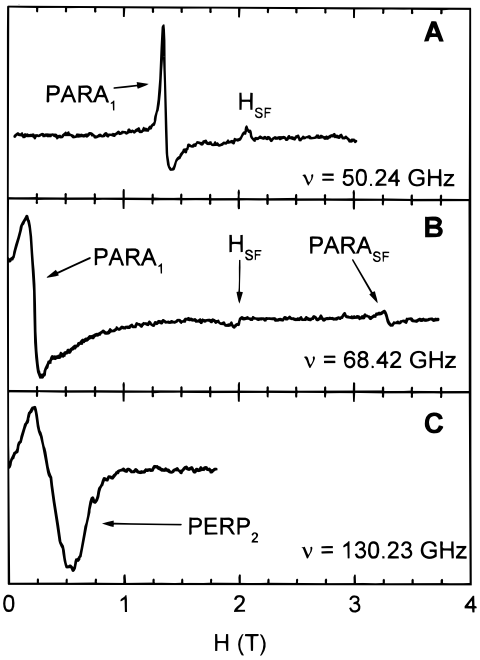

Figure 5. AFMR spectra detected for manganese hexylphosphonate at 5 K while using the MVNA source: (A) Source frequency of 50.24 GHz with signals belonging to $PARA_1$ and H_{SF}; (B) source frequency of 68.4 GHz with signals belonging to $PARA_1$, $PARA_{SF}$, and H_{SF}; (C) source frequency of 130.23 GHz with signal belonging to $PERP_2$. The signals have been scaled to show the resonances more clearly.

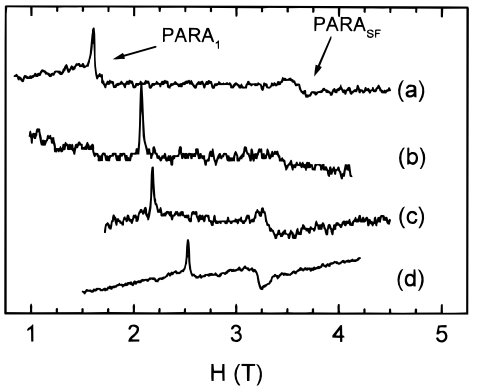

Figure 6. AFMR spectra detected at 5 K for $KMnPO_4 \cdot H_2O$ with source frequencies of (a) 61.05 GHz, (b) 50.10 GHz, (c) 45.50 GHz, and (d) 36.32 GHz. The signal originating from the $PARA_1$ branch moves to higher field as the frequency decreases, while the opposite trend is observed for the $PARA_{SF}$ signal. Signals are discussed in greater detail in the text. The signals reported are scaled to similar intensities.

measurements of the powdered samples. Figure 7 shows the results of magnetization versus field scans for each sample, with each curve vertically offset from the previous curve by 0.3 emu·G for clarity. Due to the presence of all orientations in a powdered sample, the spin-flop field, H_{SF}, does not appear as a sharp transition in the magnetization curve, but rather as a small inflection.[42] For $KMnPO_4 \cdot H_2O$, H_{SF} was 3.2 ± 0.1 T, which is higher than values of 2.3 to 2.6 T found for the manganese organophosphonates studied. These values are given for each compound in Table 1 and are in agreement with the values of the spin-flop field found from AFMR analyses.

Figure 8 shows the susceptibility versus temperature plots from 2 to 300 K for manganese pentyl- and hexylphosphonate, offset vertically by 0.1 emu/mol. The broad maximum in the temperature-dependent static susceptibility is characteristic of antiferromagnetic exchange, and the sharp change in the

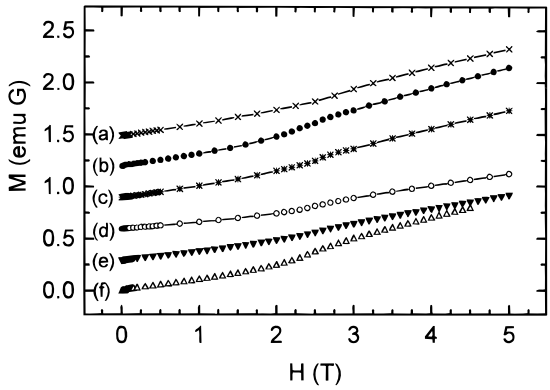

Figure 7. Magnetization versus field curves for (a) manganese phenylphosphonate, (b) manganese hexylphosphonate, (c) manganese pentylphosphonate, (d) manganese butylphosphonate, (e) manganese propylphosphonate, and (f) $KMnPO_4 \cdot H_2O$ at 2 K showing an inflection due to the spin-flop field. Curves are vertically offset by 0.3 emu·G for clarity. The solid lines are guides for the eyes and not fits to the experimental data.

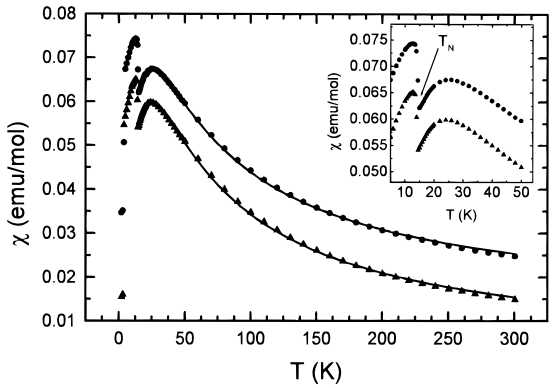

Figure 8. Magnetic susceptibility versus temperature plots for manganese pentylphosphonate (filled circles) and manganese hexylphosphonate (filled triangles) with an applied field of 0.1 T, vertically offset by 0.1 emu/mol for clarity. The solid lines are fits to the data and are discussed in the text. The data for $T < 50$ K are plotted in the inset to clearly show $T_{\chi max}$ and T_N, as discussed in the text.

susceptibility near 14 K indicates the ordering transition to the "weak ferromagnetic" state.[44] The solid lines in Figure 5 are fits between 25 and 300 K using a quadratic-layer antiferromagnet model[56] for a 2-dimensional lattice of $S = 5/2$ spins with Heisenberg antiferromagnetic nearest-neighbor exchange. The values of the nearest neighbor exchange constants, J, for manganese pentyl- and hexylphosphonate are determined from the temperature of maximum susceptibility,[42] $T\chi_{max}$, according to $|J|/2k = T_{\chi max}/2.05S(S + 1)$, and these values are included in Table 1. Values of J for the other materials are taken from literature references[34,40,42] (Table 1). Figures 9A and 10A show field cooled and zero-field cooled magnetization data over the temperature range of 2 to 25 K. The difference plots are shown in Figures 9B and 10B for the pentyl and hexyl samples, respectively. The ordering temperature, T_N, is defined as the temperature of the onset of the cusp of the magnetic susceptibility. The inset in Figure 8 and Figures 9 and 10 clearly show the cusp in the magnetic susceptibility that occurs at T_N. The values of T_N are 14.65 K for manganese pentylphosphonate and 14.10 K for manganese hexylphosphonate. Weak ferromagnetic moments of 0.044 μ_β and 0.055 μ_β, were calculated from the maximum of ΔM_{FC-ZFC}, for the pentyl and hexylphosphonates, respectively. The value of the weak ferromagnetic moments

(56) Lines, M. E. *J. Phys. Chem. Solids* **1970**, *31*, 101−116.

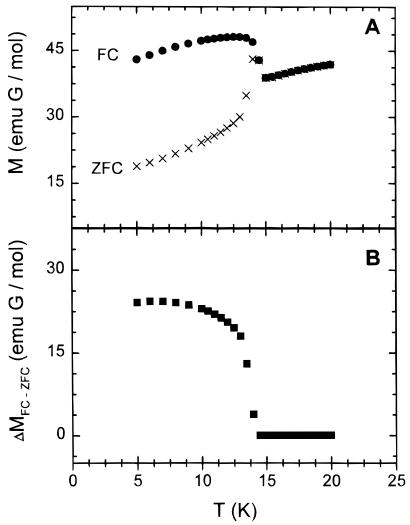

Figure 9. Magnetization versus temperature for manganese pentylphosphonate. (A) Comparison of the data taken upon warming after cooling in zero-applied field (ZFC) and cooling in an applied field (FC). In both cases, the measuring field was 0.1 T. The ordering transition, T_N, is observed as the discontinuity in the ZFC plot at 14.65 K. (B) The difference of the two plots in (A) showing the spontaneous magnetization below T_N.

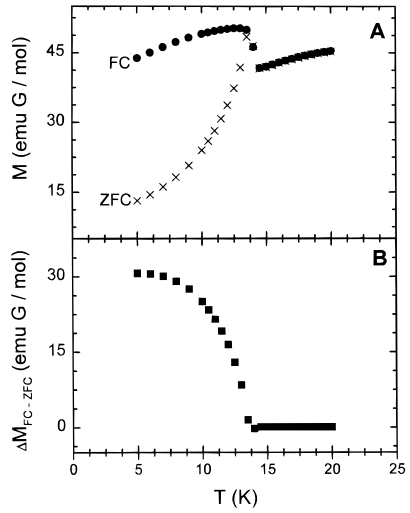

Figure 10. Magnetization versus temperature for manganese hexylphosphonate. (A) Comparison of the data taken upon warming after cooling in zero-applied field (ZFC) and cooling in an applied field (FC). In both cases, the measuring field was 0.1 T. The ordering transition, T_N, is observed as the discontinuity in the ZFC plot at 14.10 K. (B) The difference of the two plots in (A) showing the spontaneous magnetization below T_N.

determined from the magnetometry measurements are expected to represent a lower limit of the actual value (this issue is discussed in greater detail later in the text). A compilation of magnetic parameters from bulk magnetization measurements, taken from literature references[34,36,40] and from the present work are given in Table 1.

Analysis

The data shown in Figure 4, representing the observed AFMR signals in the frequency and field plane, were fit with the conventional MFT of AFMR[1−4,6,48,49] for an orthorhombic antiferromagnet modified to include a Dzyaloshinsky-Moriya interaction, H_{D-M}, as a canting term.[57,58] In the following analysis, the magnetic easy-axis is denoted by the x-direction (which corresponds to the crystallographic *b*-axis). The y- and z-directions correspond to the *ac* crystallographic plane, with the z-direction taken as the direction along which the moments cant from the easy-axis. In Figure 4A, the curve labeled $PERP_2$ corresponds to the crystallographic *c*-axis for $KMnPO_4 \cdot H_2O$ (Scheme 2), which is the direction along which the Mn $S = 5/2$ spins are canted. This branch ($PERP_2$) for the organophosphonates also corresponds to the direction of the canting moment. However, because measurements were made on powders and the relationship between the magnetic and chemical unit cells is unknown, the in-plane crystallographic orientation cannot be ascribed. The curve labeled $PERP_1$ represents the other in-plane direction perpendicular to the magnetic easy-axis, which is along the crystallographic *a*-axis in $KMnPO_4 \cdot H_2O$. The frequency and field dependence of these lines are given by:[48,57,58]

$$\mathrm{PERP}_1;\ \omega/\gamma = (H_o^{\,2} + C_1^{\,2})^{1/2} \tag{1}$$

$$\mathrm{PERP}_2;\ \omega/\gamma = (H_o^{\,2} + H_{D-M}H_o + C_2^{\,2})^{1/2} \tag{2}$$

$$C_1 = (2M_o^{\,2}(Q_x - Q_y)(A + 1/2Q_x))^{1/2} \tag{3}$$

$$C_2 = (2M_o^{\,2}(Q_x - Q_z)(A + 1/2Q_x))^{1/2} \tag{4}$$

where ω/γ is the resonance frequency, H_o is the applied field, H_{D-M} is the canting term, C_1 and C_2 are the zero-field resonance terms, all in units of Tesla (T), and with $M_o = N(g/2)\mu_\beta\langle S\rangle = 13.96$ J mol^{-1} T^{-1}. Here, C_1 and C_2 are expressed by the method of Date[48] with the removal of additional anisotropy terms (P_x, P_y, and P_z in ref 48), which were included in the original formulation of the theory to account for large orbital angular momentum contributions to the anisotropy energy. For Mn^{II}, where $S = 5/2$, contributions from orbital angular momentum can be neglected. This formalism is expressed in terms of the symmetric isotropic exchange term, *A*, and the anisotropic interaction terms, Q_x, Q_y, and Q_z, where the Q_i terms show the magnitude of the deviations from the isotropic Heisenberg limit. These terms are related to the exchange field H_E and the anisotropy fields, H_{A1} and H_{A2}, from the methods of Nagamiya, Yosida, and Kittel[1−4] by:

$$H_E = M_o A \tag{5}$$

$$H_{A1} = M_o(Q_x - Q_y) \tag{6}$$

$$H_{A2} = M_o(Q_x - Q_z) \tag{7}$$

The curve labeled $PARA_{SF}$ represents the orientation where the applied magnetic field is parallel to the magnetic easy-axis (perpendicular to the metal planes) and has a value larger than H_{SF}. The frequency and field dependence of this mode is given by:[48,57,58]

$$\mathrm{PARA}_{SF};\ \omega/\gamma = (H_o^{\,2} + H_{D-M}H_o - C_3^{\,2})^{1/2} \tag{8}$$

$$C_3 = (2M_o^{\,2}(Q_x - Q_y)(A + 1/2Q_y))^{1/2} \tag{9}$$

(57) Pincus, P. *Phys. Rev. Lett.* **1960**, *5*, 13−15.
(58) Gurevitch, A. G.; Sanina, V. A.; Golovenchitis, E. I.; Starobinets, S. S. *J. Appl. Phys.* **1969**, *40*, 1512−1517.

Table 2. Values of the Symmetric Isotropic Exchange Parameter, *A*, and of the Anisotropic Interaction Parameters, Q_x, Q_y, and Q_z, Determined from Analysis of the AFMR Signals

sample	$A \pm 0.02$ (T^2 mol/J)	$Q_x \pm 0.002$ (T^2 mol/J)	$Q_y \pm 0.001$ (T^2 mol/J)	$Q_z \pm 0.002$ (T^2 mol/J)
$KMnPO_4 \cdot H_2O$	1.33	0.022	0.003	−0.025
$Mn(O_3PC_6H_5) \cdot H_2O$	0.88	0.020	0.007	−0.027
$Mn(O_3PC_3H_7) \cdot H_2O$	1.01	0.025	0.010	−0.034
$Mn(O_3PC_4H_9) \cdot H_2O$	0.99	0.023	0.007	−0.030
$Mn(O_3PC_5H_{11}) \cdot H_2O$	1.13	0.020	0.007	−0.028
$Mn(O_3PC_6H_{13}) \cdot H_2O$	1.06	0.021	0.008	−0.030

The curves labeled $PARA_1$ and $PARA_2$ correspond to the orientation where the applied field is parallel to the magnetic easy-axis and where its value is less than that of H_{SF}. In contrast to ferromagnetic resonance[6] where there is only one parallel mode, there are two parallel AFMR modes for applied fields $< H_{SF}$ because of the presence of two sublattices. The expressions for these modes are quite complicated and are found by solving expression 16 of ref 48. A simplification of this expression was made for our system, and the resulting equations were used to fit our data (simplifications and derivation are given in the *Appendix*).

$$\mathrm{PARA}_{1\&2};\ \omega/\gamma = \{0.5\,[C_1^{\,2} + C_2^{\,2} + H_o^{\,2}(1+\lambda^2) \pm \mathrm{SQRT}\{(C_1^{\,2} + C_2^{\,2} + H_o^{\,2}(1+\lambda^2))^2 - 4(H_o^{\,2}\lambda^2 - H_o^{\,2}(C_1^{\,2} + C_2^{\,2}) + C_1^{\,2}C_2^{\,2})]\}\}^{1/2} \quad (10)$$

$$\lambda = [1 - (A + 1/2Q_x)\chi_{||}] \quad (11)$$

where λ is a variable parameter that can be used to approximate the value of $\chi_{||}$, and C_1 and C_2 are defined in eqs 3 and 4.

Generally a modified field of the type, $H_{mod} = (g/2)H_{exp}$, which accounts for the reduction of the *g*-tensor to a scalar *g*-factor is applied to the observed signals before the data can be fit with theory.[1−4] However, this modification was neglected because no anisotropy was present in the *g*-factor and the values of the *g*-factor for these materials were 2.00 ± 0.03, producing corrections that were less than the experimental error in the resonance fields, typically 0.02 to 0.1 T. However, when anisotropy of the *g*-factor is present or when its value differs significantly from 2.00, this correction must be employed.

The observed AFMR resonance signals were fit with eqs 1, 2, and 8, which provide values of H_{D-M}, C_1, C_2, and C_3. Although the canting of the sublattice magnetization vectors is too small to be determined from neutron diffraction experiments,[40] inclusion of the canting term is necessary to produce satisfactory fits of the frequency and field dependence of the AFMR signals. For the manganese phosphonates studied here, the canting term has the greatest effect on the $PERP_2$ and $PARA_{SF}$ modes in the frequency ranges of 35−70 and 120−135 GHz. The MVNA source provides access to these frequencies, making it possible to observe the effect of the canting and to determine the value of the Dzyaloshinsky−Moriya interaction. From the values of C_1, C_2, and C_3, along with the relation that $Q_x + Q_y + Q_z = 0$, eqs 3, 4, and 9 are solved to determine the values of *A*, Q_x, Q_y, and Q_z. These values are listed in Table 2. The values of the symmetric exchange field, H_E, and of the anisotropy fields, H_{A1} and H_{A2}, are listed in Table 3. The canting angle, β, is estimated from the expression:[59]

$$\tan 2\beta \cong H_{D-M}/H_E \quad (12)$$

(59) Herrmann, G. F. *J. Phys. Chem. Solids* **1963**, *24*, 597−606.

Table 3. Magnetic Parameters Determined from AFMR

sample	$H_E \pm 0.1$ (T)	$H_{A1} \pm 0.3$ (T)	$H_{A2} \pm 0.3$ (T)	$H_{SF} \pm 0.1$ (T)	$H_{D-M} \pm 0.1$ (T)	$\beta \pm 0.2$ (deg)
$KMnPO_4 \cdot H_2O$	18.5	0.26	0.65	3.1	0.5	0.9
$Mn(O_3PC_6H_5) \cdot H_2O$	12.2	0.18	0.66	2.2	0.4	0.9
$Mn(O_3PC_3H_7) \cdot H_2O$	14.1	0.21	0.82	2.3	0.3	0.7
$Mn(O_3PC_4H_9) \cdot H_2O$	13.9	0.22	0.74	2.5	0.4	0.8
$Mn(O_3PC_5H_{11}) \cdot H_2O$	15.8	0.20	0.67	2.5	0.5	0.7
$Mn(O_3PC_6H_{13}) \cdot H_2O$	14.8	0.19	0.73	2.4	0.4	0.8

and the values of H_{D-M} and β for each material are reported in Table 3.

The magnetic interaction parameters determined in the mean molecular field formalism can be related to the superexchange interactions of the spin-Hamiltonian formulation. The exchange field ($H_E = AM_o$) is related to *J* by $A = n|J|$,where *n* is the number of nearest neighbors. The anisotropy fields, H_{A1} and H_{A2}, represent both single-ion and exchange anisotropy. If the value of *J* is known independently, for example from bulk magnetization measurements, then the anisotropic exchange terms, Q_i, can be easily determined by solving eqs 3 and 4 along with the relationship $Q_x + Q_y + Q_z = 0$.[60,61] For each of the materials studied here, the values of Q_i calculated in this way were consistent with those determined from fitting the AFMR data alone.

Magnetostructural Correlations

Substituent Effects. A comparison of how the substituents influence the magnetic properties within this series of layered solids is possible because they possess nearly isostructural frameworks within the metal−oxygen−phosphorus layers. In the metal phosphonates, the layers of manganese ions are separated by the phosphonate organic groups, whereas in the purely inorganic $KMnPO_4 \cdot H_2O$, potassium ions lie in the interlayer region and the organic groups are replaced by a phosphate oxygen. Crystal structures are known for $KMnPO_4 \cdot H_2O$[40] and $Mn(O_3PC_6H_5) \cdot H_2O$,[13] and the alkylphosphonates are isostructural with these based on unit cell determinations from powder X-ray data.

The magnitude of the isotropic magnetic exchange, given by the exchange field, H_E, for the series of materials ranges from a high of $H_E = 18.5$ T for the inorganic $KMnPO_4 \cdot H_2O$ to $H_E = 12.2$ T for $Mn(O_3PC_6H_5) \cdot H_2O$, with the alkylphosphonates having intermediate values of H_E. Assuming identical superexchange pathways, the trend can be accounted for by electronic effects of the XPO_3^{2-} bridging ligands. Based on frontier orbital interaction considerations, electron-donating substituents should increase antiferromagnetic interactions mediated by the XPO_3^{2-} bridge because of a better energy match between the metal d orbitals and the bridging ligand orbitals.[62] This effect was recently demonstrated for a series of dimeric vanadyl arylphosphonates, where phosphonate-mediated superexchange increased with the electron-donating capacity of the arylphosphonate substituents.[37] For the series studied here, the electron-donating character of the substituents decreases in the order O^- > alkyl > phenyl, which is consistent with the observed trend in exchange fields of $H_E(KMnPO_4 \cdot H_2O) > H_E(Mn(O_3PC_nH_{2n+1}) \cdot H_2O) > H_E(Mn(O_3PC_6H_5) \cdot H_2O)$.

(60) A conversion factor of $N\mu_\beta^2/k = 0.325$ emu·K/mol is useful for the conversion of units between K and mol/emu.[42,61]

(61) Kahn, O. *Molecular Magnetism*; VCH: New York, 1993.

(62) Hay, P. J.; Thibeault, J. C.; Hoffman, R. *J. Am. Chem. Soc.* **1975**, *97*, 4884−4899.

Scheme 3. Representation of Exchange Pathways that Connect Each of the Mn Ions to Its Four Nearest-Neighbors[a]

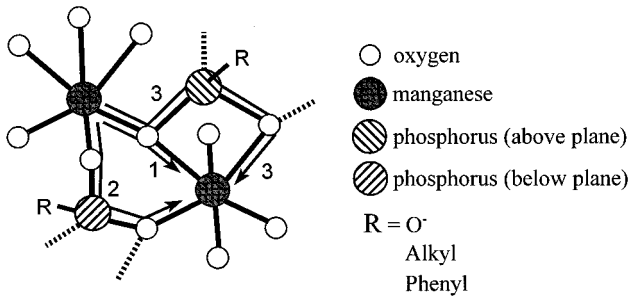

[a] The potential exchange pathways (1−3) are described in the text.

The preceding discussion assumes that the exchange pathway is the same for each member of the series. Scheme 3 depicts the three possible pathways that connect each of the manganese ions to each of its four nearest neighbors. The exchange interaction through the Mn−O−Mn bridge, labeled as pathway one, is the most direct and thought to be the dominant pathway for magnetic exchange. For $KMnPO_4 \cdot H_2O$[40] and $Mn(O_3PC_6H_5) \cdot H_2O$,[13] which have the highest and lowest exchange, the Mn−O−Mn bridging angles are similar, with values of 117.5° and 117.8°, respectively. Although the O−P−O and O−Mn−O bond angles differ, we expect these variations, that influence pathways two and three, to have little influence on the magnetic exchange by analogy with other systems.[37,63,64] In dinuclear transition metal complexes that are doubly and triply bridged by one μ−oxo bridge and one or more carboxylate or phosphonate ligands, it has been found that the carboxylate and phosphonate bridges play a negligible role as exchange pathways when compared to the bridging oxide.[63,65] Although chairlike O−P−O bridges are the sole pathways mediating magnetic exchange in materials such as $VO(O_3PC_6H_5)H_2O$,[37] this pathway requires proper symmetry and geometrical arrangements.[64] The magnitude of exchange in vanadyl phosphonates, where the exchange pathway occurs through V−O−V bridges, is much stronger than in those materials where the magnetic exchange is limited to V−O−P−O−V pathways. Hence, we expect that pathways two and three have only a small contribution to the magnetic exchange between nearest-neighbor Mn ions, and small changes in the O−P−O and O−Mn−O bond angles should not be able to account for the differences in exchange energies observed for the materials studied here. The Mn−O−Mn bond angles are nearly identical for the inorganic phosphate and phenylphosphonate samples, so the changes in exchange energies are most likely attributed to electronic perturbations of the XPO_3^{2-} bridge that result from the electron-withdrawing/donating properties of the ligand substituents.

Exchange Anisotropy. In general, the temperature at which a transition to long-range antiferromagnetic order occurs should scale with the strength of the exchange energy. In this series, the inorganic phosphate has the highest T_N (18.40 K) followed by the alkylphosphonates (14.10−15.00 K) and then the phenylphosphonate (12.1 K), and this progression is in agreement with the order of the measured exchange energies. The layered nature of these materials leads to very small interlayer exchange energies, and ordering is thought to be 2-dimensional (with subsequent 3-dimensional ordering as the temperature is lowered further[35]). The presence of Ising-type anisotropy is a requisite for long-range magnetic order in a two-dimensional lattice.[50] Although Mn^{2+} ions ($S = 5/2$) nominally experience isotropic (Heisenberg) exchange interactions, analysis of the AFMR signals reveals that magnetic anisotropy is present in the ordered state. In general, magnetic anisotropy can be considered to arise from anisotropic exchange interactions and/or single-ion anosotropy terms, and the anisotropy fields, H_{A1} and H_{A2}, in the MFT formalism of AFMR have contributions from both types of effects.[58] In the materials presented here, we are unable to separate the contributions of each type of anisotropy to the Q_i values. Therefore, the values of Q_i reported in Table 2 have contributions from both the anisotropy in the exchange and the single-ion anisotropy terms.

The magnitude of the combined anisotropy of the magnetic interactions may explain an anomaly observed in the ordering temperatures for the series of alkyl phosphonates. The manganese propyl- and butylphosphonates order at higher temperatures than the manganese pentyl and hexyl samples, although the exchange energies are larger in the latter two materials (Table 1). Analysis of the AFMR data indicates that the magnetic anisotropy [$(Q_x - Q_z)/A$ and $(Q_x - Q_y)/A$] is greater in the manganese propyl- and butylphosphonates. This larger anisotropy may be responsible for the increased ordering temperatures of the propyl- and butylphosphonates despite similar or slightly lower exchange energies. Because crystal structures are not available for the series of alkylphosphonates, we cannot unambiguously identify the subtle structural changes that are responsible for the differences observed in the magnetic parameters. However, assuming the same intralayer spacing of the XPO_3^{2-} ligands in the alkylphosphonates that are present in the phenylphosphonate, van der Waals interactions between adjacent alkyl groups are expected to become important for alkyl chain lengths greater than four carbons.[13] It is not unreasonable to infer that subtle structural differences exist between the shorter chain propyl- and butylphosphonates and the longer chain pentyl- and hexylphosphonates.

Canting Moments. There are two kinds of anisotropic coupling mechanisms that can produce canting of the sublattice magnetization vectors.[42,44,58,66] Antisymmetric exchange, which is proposed to occur for a variety of site symmetries and which operates in addition to symmetric Heisenberg exchange, is described by:

$$H_{aniso} = \mathbf{d}[S_1 \times S_2]$$

where **d** is a constant vector that depends on the symmetry of the crystal. This type of interaction is seen in α-FeO_3 and is often referred to as a Dzyaloshinsky−Moriya vector.[43,44,57] The other mechanism, as seen in NiF_2 and related crystals, is single-ion magnetocrystalline anisotropy energy,[66] which results when there are two equivalent sites of magnetic ions but the directions of their anisotropy axes are different. In the metal organophosphonates, because the symmetry of the space group $Pmn2_1$ is sufficiently low, it is believed that the first mechanism operates and antisymmetric exchange is responsible for the spontaneous magnetization in these materials.[34]

The Dzyaloshinsky−Moriya exchange term, H_{D-M}, was determined from fitting the $PERP_2$ and $PARA_{SF}$ modes with eqs 2 and 8, respectively. Although the canting of the sublattice magnetization vectors was too small to be detected in neutron diffraction experiments on $KMnPO_4 \cdot H_2O$, inclusion of the

(63) Norman, R. E.; Yan, S.; Que, J. L.; Backes, G.; Ling, J.; Sanders-Loehr, J.; Zhang, J. H.; O'Conner, C. J. *J. Am. Chem. Soc.* **1990**, *112*, 1554−1562.

(64) Beltran-Porter, D.; Amoros, P.; Ibanez, R.; Martinez, E.; Beltran-Porter, A.; Le Bail, A.; Ferey, G.; Villeneuve, G. *Solid State Ionics* **1989**, *32/33*, 57−69.

(65) Weihe, H.; Gudel, H. U. *J. Am. Chem. Soc.* **1997**, *119*, 6539−6543.

(66) Moriya, T. *Phys. Rev.* **1960**, *117*, 635−647.[42,61]

canting term in the AFMR analysis was necessary to produce satisfactory fits to the experimental data. The values of β for each material, which are listed in Table 3, show that the canting angle was quite similar for all of the materials and that its value ranged from 0.7 to 0.9 ± 0.2°. Apparently the strength of this interaction in these materials is not directly affected by the identity of the phosphate/phosphonate substituent. This result is in contrast to the estimates of the canting angle determined from SQUID magnetometry measurements that show that the values of the canting angle (denoted by α in Table 1) are 2−5 times smaller than those determined from the AFMR measurements (denoted by β in Table 3) and that these values change as the phosphonate substituent is varied. However, because these materials are powdered, magnetization measurements are a statistical average over all particle orientations, and estimates of the canting moment obtained in this way are lower than the canting moments measured by AFMR. Also, the varied estimates of the canting moment obtained from magnetization measurements may result from contributions of uncompensated spins at domain boundaries as well as having contributions from inhomogeneous sample packing because of irregular particle size and shape. The canting angles determined from AFMR are not affected by sample packing because H_{D-M} is determined by the energy of the AFMR modes and not the intensities. It is worth noting that had single crystals been available for this study, AFMR could have observed not only the magnitude, but also the direction of the spin canting.

Conclusions

AFMR provides a microscopic probe of antiferromagnetic materials. The high field EMR facilities at NHMFL, with field sweep capabilities from 0 to 17 T, the availability of several frequency sources, and variable temperature capabilites, make this technique applicable to a wide range of materials. Here we have shown how AFMR can be easily used to compare the magnetic parameters of chemically similar materials. Some of the advantages of AFMR over other microscopic probes have been demonstrated, including high sensitivity to subtle differences in magnetic interactions and the ability to work with a small amount of material.

Measurements performed on $KMnPO_4 \cdot H_2O$, a series of manganese alkylphosphonates [$Mn(O_3PC_nH_{2n+1}) \cdot H_2O$; n = 3−6], and manganese phenylphosphonate [$Mn(O_3PC_6H_5) \cdot H_2O$] reveal that although the magnetic structures are similar among these materials, differences can be detected using AFMR. Because the superexchange pathways in these materials are nearly identical, the observed differences in the magnetic exchange are thought to arise from electronic perturbations caused by the phosphate/phosphonate substituents. It was observed that the symmetric exchange field decreased as the electron-donating ability of the substituent decreased, following the trend $H_E(KMnPO_4 \cdot H_2O) > H_E(Mn(O_3PC_nH_{2n+1}) \cdot H_2O) > H_E(Mn(O_3PC_6H_5) \cdot H_2O)$. Analysis of the frequency and field dependence of the AFMR signals revealed that the canting angle, β, for these materials was 0.7−0.9 ± 0.2°. In addition, the anisotropy of the magnetic interactions is determined from analysis of the frequency and field dependence of the AFMR signals. The values of the exchange field determined from the AFMR mean molecular field formulation, can be related to the value of the superexchange constant, J, determined from magnetic susceptibility measurements.

Appendix

For orthorhombic antiferromagnets, eqs 11 and 12 relate the frequency and field dependence of the two parallel AFMR signals when the applied field has a value less than the spin-flop field. These expressions are derived from a simplification of expression 16 of ref 48. The first simplification is the assumption that $P_x \cong P_y \cong P_z \cong 0$. This approximation is justified from both experimental and theoretical considerations. The original formulation of this theory was for the treatment of AFMR of $CoCl_2 \cdot 6H_2O$, where a second rank tensor **P** was included in the exchange energy expression to account for contributions to the anisotropy energy originating from orbital angular momentum. For our system of Mn^{II}, where $S = 5/2$, it is expected that these effects would be minimal. In addition, if $P_i \neq 0$, fits to the AFMR signals for $PERP_1$, $PERP_2$, and $PARA_{SF}$ (eqs 1, 2, and 8) would have included a nonunity coefficient in front of the H_o^2 term (see eqs 18 and 19 of ref 48). Because a nonunity coefficient of the H_o^2 term in these expressions was not necessary to fit our data, this simplification is justified. The second simplification made was the assumption that $A - 1/2Q_z = A + 1/2Q_y = A + 1/2Q_x$ ($A \gg Q_i$), which allowed for the reduction of the expression to a quadratic form. The new matrix expression with $\lambda = [1 - (A + 1/2Q_x)\chi_{||}]$ now becomes:

$$\begin{bmatrix} \frac{-i\omega}{\gamma} & H & 0 & (Q_x - Q_z)M_0 \\ -H & \frac{-i\omega}{\gamma} & (Q_y - Q_x)M_0 & 0 \\ 0 & 2(A+1/2Q_x)M_0 & \frac{-i\omega}{\gamma} & H\lambda \\ -2(A+1/2Q_x)M_0 & 0 & -H\lambda & \frac{-i\omega}{\gamma} \end{bmatrix} = 0 \quad \text{(A1)}$$

Simplification gives a quadratic equation with solutions:

$$\omega/\gamma = \{0.5\,[C_1^2 + C_2^2 + H_o^2(1+\lambda^2) \pm [\{(C_1^2 + C_2^2 + H_o^2(1+\lambda^2))^2 - 4(H_o^2\lambda^2 - H_o^2(C_1^2 + C_2^2) + C_1^2C_2^2)]\}]^{1/2}\}^{1/2} \quad \text{(A2,10)}$$

where C_1 and C_2 are the zero-field resonance terms and are given in the text by eqs 3 and 4. For simplicity, because the H_{D-M} interaction is expected to have only small perturbations on the energies of the $PARA_1$ and $PARA_2$ modes, for these materials this interaction was not included in the calculation of the frequency and field dependence of these modes.

Acknowledgment. The authors acknowledge the National Science Foundation, DMR-9530435, for financial support and the NHMFL In-House Research Program for support of the Tallahassee operations. We thank Prof. K. Katsumata for informative discussions that introduced us to the technique of AFMR. We thank Prof. J. R. Childress for making the SQUID magnetometer available for our use (acquired through an NSF instrumentation grant, DMR-9422192).

JA974247G